WILEY | Hindawi

Research Article

Three-Dimensional Poincaré Plot Analysis for Heart Rate Variability

Bin Wang [iD],[1,2] **Dewen Liu** [iD],[1] **Xin Gao** [iD],[1] **and Yunlei Luo** [iD][1]

[1]*School of Physics and Electronic-Electrical Engineering, Ningxia University, Yinchuan 750021, China*
[2]*New Energy (Photovoltaic) Industry Research Center, Qinghai University, Xining, Qinghai 810000, China*

Correspondence should be addressed to Bin Wang; wangbin053@nxu.edu.cn

For the limitation of Poincaré plot analysis, the three-dimensional Poincaré plot analysis is proposed to analyze the heart rate variability. Firstly, the Poincaré plot and some classic indicators are briefly discussed. Because the standard analysis method inherently ignores the embedding temporal information of the RR interval time series, the temporal variation of the time series cannot be adequately reflected. Secondly, for the limitation of the Poincaré plot analysis, a three-dimensional Poincaré plot is presented, which can fully describe the temporal and spatial characteristics of the RR interval time series. Thirdly, we propose the local distribution entropy, which can quantify the temporal and spatial patterns of the scatter points in novel space. Finally, PhysioNet/PhysioBank is applied in this study. The experimental results demonstrate the effectiveness of the three-dimensional Poincaré plot analysis.

1. Introduction

Heart rate variability (HRV) is the variation in the beat-to-beat timing of the heart, which has a close relation with the autonomic nervous system (ANS) [1]. Through cardiovascular disease research, the interactions of the sympathetic nervous system (SNS) and the parasympathetic nervous system (PNS) have been adequately studied. Research shows that many heart diseases can result in the obvious variation of the SNS and PNS activity universally, which can be directly reflected by the HRV. Thus, HRV is often used to evaluate the state of the cardiovascular system. As a significant prognostic indicator, the time and frequency characteristics of the HRV have been extensively researched. In 1963, the clinical significance of HRV was firstly used by Hon and Lee [2], who noted that fetal distress was accompanied by changes in interbeat intervals.

As a significant tool, the Poincaré plot is widely applied to analyze the HRV. Various distributions of scatter points derived from the RR interval time series represent the corresponding physiology status and the distribution pattern of points can provide a wealth of physiological information

of the cardiovascular system [3]. For instance, the Poincaré plot of healthy humans is an approximate ellipse. To analyze the distribution pattern objectively and extract physiological information from the cloud of points quantitatively, in the past decade, many indicators are presented [4–8] and are applied in various detections of cardiovascular diseases [9–15]. The Poincaré plot is an effective analytical method for heart rate variability. Via the tool, the RR interval time series can be visualized in a two-dimensional coordinate system. As the basic indicators, the minor and major axes of the fitted ellipse (SD1, SD2) [4] are extensively used to estimate the morphology of the fitted ellipse, which partly represents the short-term and the long-term HRV. The fitted ellipse area of scatter points (S) [5] is another basic indicator, which reflects the degree of dispersion of the points and depicts the level of variation of the HRV.

In the Poincaré plot, all scatter points are divided into two parts by the main diagonal. As the RR intervals are nonlinear time series, the numbers of these scatter points in the two areas are inequal and the unbalanced distribution of points contains a great deal of physiological information. The asymmetry of the distribution for these scatter points is

measured by some typical asymmetry indexes, such as Ehler index (EI) [6], Guzik index (GI) [7], and Porta index (PI) [8]. Based on the Poincaré plot, the RR interval time series in the form of the scatter points is reconstructed in two-dimensional space, whereas the temporal information contained in the RR time series is inherently ignored by the Poincaré plot and those basic indicators.

The study of feature extraction via the Poincaré plot is a continuation of our preliminary research [16–20]. Aiming at the limitation of the classic Poincaré plot, two crucial problems need to be solved. The first is how to reasonably represent the temporal characteristic and the spatial distribution of scatter points in three-dimensional space. In the study, the time element of scatter points will be embedded in the standard Poincaré plot. We expect that based on the improved Poincaré plot, the temporal and spatial characteristics of the RR interval time series would be fully described. The second is how to reasonably calculate the temporal–spatial information of scatter points in the improved Poincaré plot. Here, in the novel coordinate system, the space is divided into several subspaces. By calculating the entropy of all subspaces, we hope to obtain a rational evaluation value for a certain pattern of scatter points. the main contributions of this study are as follows:

(1) We propose a three-dimensional Poincaré plot (TDPP). Based on the TDPP, the RR interval time series is reconstructed and the physiological status of the heart can be comprehensively reflected.

(2) The local distribution entropy (LDE) is presented, which is applied to measure the distribution of scatter points in the TDPP.

(3) In the study, five datasets and six indicators are being used to validate our method. The experiment's results illustrate that the TDPP and LDE are effective and the performance of the algorithm is relatively stable.

The arrangement of this paper is organized as follows: The Poincaré plot and the conventional descriptors are briefly introduced in Section 2. Section 3 provides the three-dimensional Poincaré plot and the local distribution entropy in detail. In Section 4, experiments are given to demonstrate the performance of our method. The main conclusions are given in Section 5.

2. Poincaré Plot Analysis

In this section, we will review the theory of the Poincaré plot and several basic descriptors briefly. Meanwhile, the limitations of the Poincaré plot analysis will be discussed.

2.1. Poincaré Plot. Poincaré plot is a nonlinear and geometrical analysis method for HRV, which can reconstruct the RR interval time series in two-dimensional space. Via the Poincaré plot, the time series in the form of scatter points is distributed in a plane, which intuitively shows abundant distribution patterns. The theoretical foundation of the Poincaré plot is the Takens theorem [21].
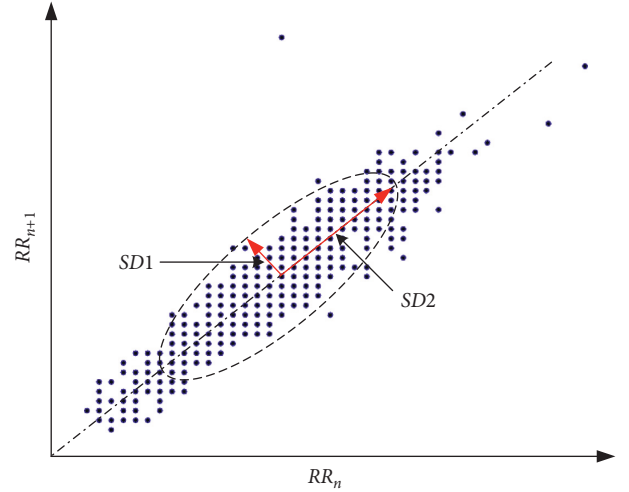

Figure 1: Standard Poincaré plot. SD1 and SD2 are the minor and major axes of the fitted ellipse, respectively.

Based on the theory, the dynamic characteristic of the heart is reconstructed appropriately in a bidimensional phase space by a given time delay. In Figure 1, for the Poincaré plot of HRV, the coordinate values of the scatter points are described by two consecutive RR intervals. The x-coordinate and the y-coordinate of the scatter points are RR_i and RR_{i+1}, respectively, where RRi is the ith time interval. Various distribution patterns of scatter points represent different physiological states of the heart; for instance, in general, a healthy human's heart status is comet-shaped, a heart failure patient's pattern is fan-shaped, an artificial pacemaker of the heart rate's pattern is round, etc.

2.2. Quantitative Indicators. In recent decades, a large number of indicators were proposed to recognize the distribution pattern of scatter points quantitatively. In the Poincaré plot, the scatter points can be fitted to an ellipse. The half minor axis (SD1) and the half major axis (SD2) of the ellipse are the most important quantitative indicators.

$$SD1 = \sqrt{\frac{1}{N-1} \sum_{i=1}^{N-1} \frac{\left(RR_i - RR_{i+1}\right)^2}{2}},$$

$$SD2 = \sqrt{\frac{1}{N-1} \sum_{i=1}^{N-1} \frac{\left(RR_i + RR_{i+1} - 2\overline{RR}\right)^2}{2}}, \quad (1)$$

where N is the length of the RR interval time series and $\overline{RR}$ denotes the mean of the time series. The indicator SD1 is the minor axis of the fitting ellipse, which represents the variation in the two successive RR intervals. The other indicator SD2 reflects the range of the RR intervals. Based on the basic indicators, the degree of dispersion of scatter points quantitatively is objectively estimated and the variation of the HRV is reflected indirectly.

In addition, the area of the fitted ellipse (S) is a useful indicator to detect the distribution pattern.

$$S = \pi \times SD1 \times SD2. \tag{2}$$

In the Poincaré plot, the main diagonal divides the plane into two parts. The number of points in the two regions is usually unequal. Thus, many studies have focused on the asymmetric indicators of the Poincaré plot. These typical indicators are listed as follows.

The Porta indicator (*PI*) is used to calculate the proportion of points in different parts.

$$PI = \frac{C\left(P_i^-\right)}{C\left(P_i^+\right) + C\left(P_i^-\right)}, \tag{3}$$

where $C\left(P_i^+\right)$ denotes the number of points above the main diagonal and $C\left(P_i^-\right)$ is the number of points below the main diagonal.

The Guzik indicator (*GI*) depicts the asymmetry of distribution through the proportion of distances of the points from the main diagonal.

$$GI = \frac{\sum_{i=1}^{C\left(P_i^+\right)}\left(D_i^+\right)^2}{\sum_{i=1}^{N-1}\left(D_i^+\right)^2}, \tag{4}$$

where D_i^+ is the distance of the ith point above the main diagonal from the main diagonal, D_i is the distance of the ith point from the main diagonal, and N is the number of scatter points.

The Ehler indicator (*EI*) calculates the degree of asymmetry of distribution by the first difference of consecutive RR intervals.

$$EI = \frac{\sum_{i=1}^{N-1}\left(RR_i - RR_{i+1}\right)^3}{\left(\sum_{i=1}^{N-1}\left(RR_i - RR_{i+1}\right)^2\right)^{3/2}}. \tag{5}$$

Although many quantitative analysis indicators of the standard Poincaré plot have been presented to identify the distribution patterns of scatter points, they still have some primary limitations. In the Poincaré plot, the coordinates of the scatter points are composed of two consecutive RR intervals, respectively. The spatial locations of consecutive scatter points contain a great deal of temporal information, which is an important information source to recognize the cardiovascular disease. However, as mentioned earlier, these basic and asymmetric indicators only focus on the spatial distribution of scatter points, and the temporal information of the RR interval time series is inherently ignored.

To overcome the limitations of the standard Poincaré plot analysis, the improved analysis method is given in the next section.

3. Three-Dimensional Poincaré Plot Analysis

In the study, the standard Poincaré plot is modified properly. We set a new coordinate axis, *z*-axis, that is perpendicular to the plane of the standard Poincaré plot. In the space of the improved Poincaré plot, the physiological states of the heart can be shown adequately.

In Figure 2, the coordinates of the three points P_i, P_{i+1}, and P_{i+2} are (RR_i, RR_{i+1}), (RR_{i+1}, RR_{i+2}), and (RR_{i+2}, RR_{i+3}),
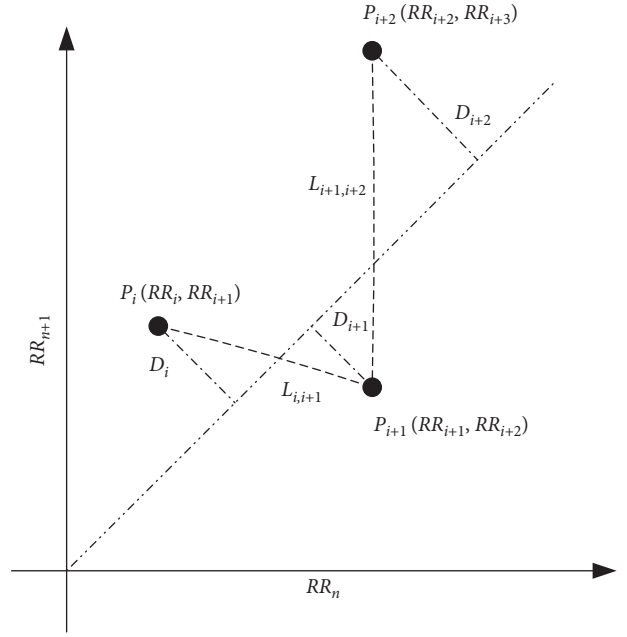

Figure 2: The positional relationship of consecutive points in the Poincaré plot.

respectively. We can find that the y-coordinate of P_i is the same as the x-coordinate of P_{i+1}. Hence, the symmetry of the two points on the side of the main diagonal depends on the x-coordinate of P_i and the y-coordinate of P_{i+1}. Actually, the symmetry of two successive data points well depicts the difference between the two RR intervals RR_i and RR_{i+2} from another perspective. The symmetry of the two points can be calculated by the parameter *L*.

$$L_{i,i+1} = \left|RR_i - RR_{i+2}\right|, \tag{6}$$

where RR_i is the x-coordinate of P_i and RRi+2 is the y-coordinate of P_{i+1}. The value of $L_{i,i+1}$ reflects the variation of the HRV to a certain extent.

On the other hand, because the coordinates of a scatter point are the consecutive *RR* intervals, the difference between the horizontal and vertical coordinates of the point reflects the change of consecutive *RR* intervals RR_i and RR_{i+1} in essence. The more the distance *D*, the more the difference between RR_i and RR_{i+1} is significant. In other words, the value of *D* is in a positive correlation with the magnitude of change between two consecutive RR intervals. In addition, the degree of the variation can be quantified by distance *D* further.

$$D_i = \frac{\left|RR_i - RR_{i+1}\right|}{\sqrt{2}}, \tag{7}$$

where D_i is the distance from point P_i to the main diagonal, and RR_i and RR_{i+1} are the horizontal and vertical coordinates, respectively.

The two parameters D_i and *L* reflect the variation of the HRV partly, which will be used to describe the embedding temporal information of the RR interval time series.

In the study, we build a *z*-axis that is perpendicular to the plane of the standard Poincaré plot and the RR interval time
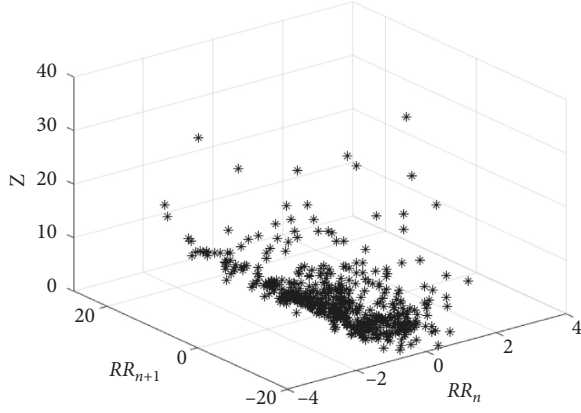
FIGURE 3: Three-dimensional Poincaré plot of No. nsr001, derived from the normal sinus rhythm RR interval database.

series is reconstructed in a three-dimensional Poincaré plot. In Figure 2, the z-coordinate of the scatter point P_{i+1} can be calculated as

$$Z_{i+1} = L_{i+1}(D_{i+1} + \varepsilon),\tag{8}$$

where $L_{i+1} = \sqrt{L_{i,i+1}^2 + L_{i+1,i+2}^2}$. In the Poincaré plot, some points may be on the main diagonal and the parameters D_i of these points are zero. We add a parameter ε in the equation to avoid this case. Here, the parameter ε is set to 0.01. In the TDPP, the coordinates of the point P_{i+1} are (RR_{i+1}, RR_{i+2}, Z_{i+1}).

As we know, the points are distributed in the first quadrant of the Poincaré plot and they are usually near the main diagonal. With the distribution position of these points, it is difficult to calculate the various quantitative indicators. To facilitate the calculation of these indicators, we hope that the center of the fitting ellipse of all data points moves to the origin of the Poincaré plot and the major axis of the ellipse overlaps the x-axis of the Poincaré plot by the transformation of coordinates. Here, the coordinates of the point in the TDPP are rotated clockwise by 45°. The rotated coordinates are calculated as

$$\begin{bmatrix} RR_{i+1}' \\ RR_{i+2}' \\ Z_{i+1} \end{bmatrix} = \begin{bmatrix} \cos 45° & -\sin 45° & 0 \\ \sin 45° & \cos 45° & 0 \\ 0 & 0 & 1 \end{bmatrix} \begin{bmatrix} RR_{i+1} - \overline{RR_n} \\ RR_{i+2} - \overline{RR_{n+1}} \\ Z_{i+1} \end{bmatrix},\tag{9}$$

where $\overline{RR_n}$ and $\overline{RR_{n+1}}$ are the means of the x-axis and y-axis of all scatter points, respectively. Then, the new coordinates of P_{i+1} are (RR_{i+1}', RR_{i+2}', Z_{i+1}).

An example of a TDPP is shown intuitively in Figure 3. The distribution pattern of the standard Poincaré plot is fully reserved in the point projections of the lower end of the space. Meanwhile, the z-coordinates of the scatter points well quantize the change of the consecutive RR intervals and provide a large amount of time information of the RR interval time series.

Compared with the standard Poincaré plot, in the TDPP, the potential temporal and spatial characteristics of the time series can be shown more comprehensively. Nevertheless, how to analyze the HRV in the TDPP is another crucial problem. In this study, the local distribution entropy is
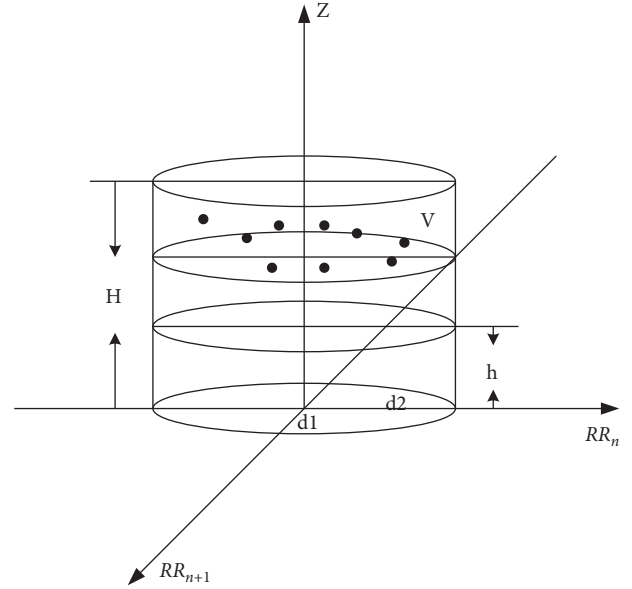

FIGURE 4: The space division of the TDPP.

proposed, which can calculate the temporal and spatial characteristics of the scatter points quantitatively. Specifically, the three-dimensional space of the TDPP is divided into several subspaces. The LDE can be calculated by the number of points in every subspace.

In Figure 4, the distribution patterns of all points are analyzed in an elliptical cylinder. For the enclosed space, the maximum value of the z-coordinate of all scatter points is selected as the height. The upper and lower ends of the space are an ellipse, which is fitted in the standard Poincaré plot. The maximum coordinates of the x-coordinate and the y-coordinate of all scatter points are chosen as the major axis and the minor axis of the ellipse, respectively. The elliptical cylinder is divided into several subspaces further in order to analyze data distribution in detail. In Figure 4, there are three subspaces with the height of the subspace being h, in which we can calculate the LDE by counting the points of the subspace.

The concept of entropy in information theory is usually used to calculate the complexity of the dynamic system. In this paper, based on the TDPP and the concepts of entropy, a novel indicator of local distribution entropy that can estimate the variation levels of HRV is proposed. It is defined as follows:

$$p_i = \begin{cases} \dfrac{\min(s_i, h_i)}{\max(s_i, h_i)} \times \dfrac{|s_i + h_i - \overline{m}|}{M}, & \min(s_i, h_i) \neq 0, |s_i + h_i - \overline{m}| \neq 0, \\[3mm] \dfrac{|s_i + h_i - \overline{m}|}{M}, & \min(s_i, h_i) = 0, |s_i + h_i - \overline{m}| \neq 0, \\[3mm] l, & |s_i + h_i - \overline{m}| = 0, \end{cases}\tag{10}$$

$$E_L = \sum_{i=1}^{N} - p_i \log(p_i),\tag{11}$$

where N is the number of subspaces, M is the number of all points in the TDPP, $\overline{m}$ is the average number of the scatter points in every subspace, l is a constant, and s_i and h_i are the number of scatter points that possess negative and positive values of the y-coordinate in the ith subspace, respectively. In the formula (10), $\min(s_i, h_i)/\max(s_i, h_i)$ is a ratio of s_i and h_i in the ith subspace, which reflects the equilibrium of the scatter point distribution on both sides of the x-axis and describes the degree of variation of the heart rate. Furthermore, $|s_i + h_i - \overline{m}|/M$ depicts the relationship between the number of points in the ith subspace and the mean value $\overline{m}$. Based on the distribution of the points, the parameter p_i is selectively calculated under three conditions. Firstly, the pi is calculated under the first case if the points are distributed over both sides of the y-axis and the number of the points in a subspace is unequal to the average of the points in every subspace. Secondly, if only the points in the subspace are located on one side of the y-axis, the parameter will be computed under the second case. Finally, p_i is set to be a constant l if the number of points in the subspace is equal to the average $\overline{m}$. Based on the formula (10), we can find that the parameter p_i is restricted by $\min(s_i, h_i)/\max(s_i, h_i)$ and $|s_i + h_i - \overline{m}|/M$. If there is a significant difference in the number of points on both sides of the x-axis or the number of the points in the ith subspace is closer to the mean value, the parameter p_i is closer to zero. In the formula (11), EL is the sum of the entropy of all subspaces, which can reflect the variation levels of the HR as a whole. From a macro perspective, if the variation level of the HR is higher, the points in the TDPP are more likely to be distributed in every subspace and we could obtain a larger LDE. On the other hand, if most of the points are located in the "lower" subspaces, the indicator LDE will be smaller.

In conclusion, theoretically, a three-dimensional Poincaré plot analysis can ensure that the temporal and spatial characteristics of HR are adequately shown and properly measured.

In order to extract the features of HRV more effectively, the RR interval time series needs to be preprocessed by the moving average filter.

$$\widetilde{RR}(i) = \sum_{i=1}^{N-\tau} \sum_{j=0}^{\tau-1} \left(RR_{i+j+1}/\tau \right), \qquad (12)$$

where N is the length of the time series and τ is the size of the moving window.

Now, the steps of the three-dimensional Poincaré plot analysis are listed as follows:

(1) The *RR* interval time series is processed by equation (13).

(2) Via the preprocessed *RR* interval time series, construct the scatter points of the standard Poincaré plot $\{P_1, P_2, \ldots, P_n\}$. The coordinates of the point p_i are (RR_i, RR_{i+1}).

(3) Calculate the symmetry parameter $L_{i,i+1}$ by Equation (7) and the Euclidean distance D_i by Equation (8).

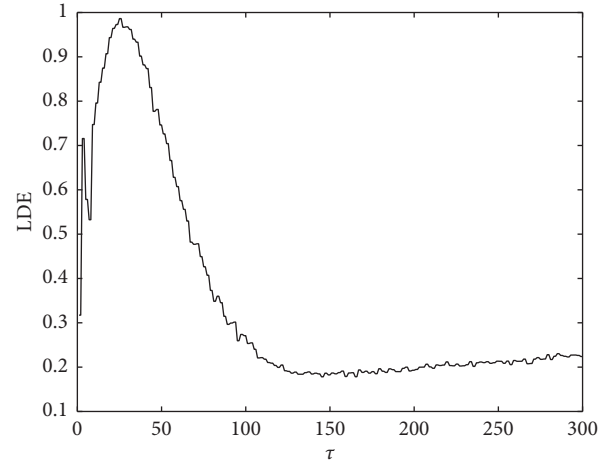(4) Compute the z-coordinate of the point by Equation (9).

FIGURE 5: LDE of nsr2db with the changed moving window width τ.

(5) Transform the coordinates of scatter points by Equation (10).

(6) Divide the elliptical cylinder into several subspaces and calculate the LDE by Equations (11) and (12).

In this section, the algorithm of the three-dimension Poincaré plot analysis is adequately introduced. In the next section, our method is applied in several cardiovascular diseases and the performance of the algorithm is further illustrated.

4. Application of the Three-Dimensional Poincaré Plot Analysis

As an important database, PhysioNet/PhysioBank contains over 36000 recordings of physiological signals and time series, which has been widely used in the field of biological signal analysis. In this section, five databases, Normal Sinus Rhythm RR Interval Database (nsr2db) [22], MIT-BIH Arrhythmia Database (mitdb) [23], Post-lctal Heart Rate Oscillations in Partial Epilepsy (szdb) [24], CU Ventricular Tachyarrhythmia Database (cudb), and Sudden Cardiac Death Holter Database (sddb) [22], are used to assess the performance of the three-dimensional Poincaré plot analysis. In this experiment, all physiological signals need be processed by three steps: Firstly, to highlight the characteristics of the RR interval time series, each experimental dataset is preprocessed by a moving average filter. Secondly, based on the Takens theorem, the filtered data are used to construct the Poincaré plot. Thirdly, via the constructed points, the parameters $L_{i,i+1}$, D_i, z-coordinate, and LDE are calculated.

In Section 4.1, the moving window width of the filter and the number of subspaces of the TDPP will be chosen objectively. Via the five databases, the performance of the algorithm will be further illustrated in Section 4.2.

4.1. Parameter Setting. To highlight the biological features of the processed signals, the moving average filter is applied to

TABLE 1: Results of the *t*-test between nsr2db and the other four datasets, cudb, mitdb, sddb, and szdb.

Number of subspaces	*p* value			
	nsr2db, cudb	nsr2db, mitdb	nsr2db, sddb	nsr2db, szdb
10	1.87×10^{-15}	5.34×10^{-24}	0.8878	7.59×10^{-4}
50	1.21×10^{-29}	1.36×10^{-40}	0.1026	1.09×10^{-4}
100	3.79×10^{-33}	1.08×10^{-39}	0.0034	2.64×10^{-4}
150	4.83×10^{-34}	1.01×10^{-37}	1.91×10^{-4}	1.60×10^{-4}
200	2.68×10^{-37}	1.53×10^{-36}	5.84×10^{-5}	1.88×10^{-4}
250	1.81×10^{-35}	3.07×10^{-36}	2.63×10^{-6}	1.46×10^{-4}
300	9.88×10^{-37}	1.77×10^{-35}	1.13×10^{-6}	1.36×10^{-4}
350	9.88×10^{-37}	1.77×10^{-35}	1.13×10^{-6}	1.36×10^{-4}

preprocess the raw RR interval time series. Choosing a reasonable moving window width is a key problem for the preprocess.

In this subsection, nsr2db is applied to choose the moving window width τ, which includes 54 long-term ECG signals of the normal sinus rhythm. In the dataset, the ECG signal is digitized at 128 samples per second and noted by automated analysis with manual review and correction.

Figure 5 shows the sensitivity of the LDE with the changed moving window width τ. The number of subspaces is preliminarily set to 20. The experimental results show that there are some larger LDEs when the parameter τ changes in the interval [17, 37]. Hence, in this experiment, the parameter τ is set to 25.

Based on the novel analysis method, all reconstructed scatter points are fully interspersed in the TDPP. By counting the points in each subspace, the distribution of the points can be well estimated quantitatively. Therefore, the number of subspaces in the TDPP is closely related to the value of the LDE, which needs to be chosen properly.

Table 1 shows the LDEs of the *t*-test with different number of subspaces. For the two datasets nsr2db and cudb, the LDEs of the *t*-test decrease gradually with the number of subspaces increasing. The *t*-test results of the nsr2db and sddb are similar to the case of nsr2db and cudb largely. For the other datasets, nsr2db and szdb, the table shows that the *t*-test results have no significant variation. It is interesting that for nsr2db and mitdb, the change in the *t*-test results increases gradually. Given the amount of computation and the precision of our algorithm, in this study, the number of subspaces of the TDPP is set to 200.

4.2. Performance Comparison. To validate that a healthy human can be more easily identified from a human who suffers from cardiovascular diseases via our algorithm, six classic indicators of the Poincaré plot are adopted in this experiment. Through the difference of experimental results between nsr2db and the other four datasets, the performance of these indicators can be tested intuitively.

Figure 6 shows the results of the seven indicators for the five datasets. (a)~(g) are the boxplots of the indicators SD1, SD2, S, EI, GI, PI, and LDE, which can integrally describe the numerical range of the experimental results. In Figure 6(a), the experimental results of SD1 show that there is a considerable overlap between the box (interquartile range) of nsr2db and the whisker (upper quartile) of cudb. In Table 2,

the means and standard deviations of nsr2db and cudb are 101.41 ± 0.64 and 92.73 ± 25.20, respectively. Similarly, the box of nsr2db and the lower quartile of whisker of mitdb are overlapping completely and the numerical range of them are 101.41 ± 0.64 and 103.33 ± 3.82. As a descriptor of the standard Poincaré plot, the overlapping of numerical ranges indicates that the normal sinus rhythm can hardly be identified from the other two subjects, ventricular tachyarrhythmia and arrhythmia. Different from the above cases, the boxes of nsr2db and the other two datasets, sddb and szdb, are non-overlapping completely and their numerical ranges are 101.41 ± 0.64, 105.29 ± 0.53, and 104.72 ± 0.67, respectively. The results mean that the indicator has the ability to recognize the normal sinus rhythm from epilepsy and sudden cardiac death.

Analogously, the classification capacity of the other five indicators, SD2, S, EI, GI, and PI, is shown intuitively in Figures 6(b)–6(f). We find that there are some numerical range overlaps between nsr2db and the other four datasets, which illustrates that these descriptors cannot differentiate the normal sinus rhythm from the other four subjects.

For the novel indicator LDE, the experimental results are shown in Figure 6(g) and Table 2. Compared to the numerical ranges of all results, there is non-overlapping between nsr2db and the other four datasets totally. The mean of the experimental result of nsr2db is higher than the others obviously. The results indicate that as an effective feature of HR, LDE can be used to recognize the normal sinus rhythm from the four arrhythmia subjects. Compared to other classic indicators, the performance of our method is more stable. The presented experimental results show that only LDE can successfully recognize the normal from the other four pathologies.

As a common classification algorithm, the k-means algorithm is preliminarily applied to recognize the normal sinus rhythm from the other four datasets via the seven indicators, thereby demonstrating the effectiveness of our method. In the clustering experiment, *RI* is used to assess the performance of the aforementioned indicators. The *RI* is defined as

$$RI = \frac{CD}{TD}, \tag{13}$$

where *CD* is the number of correct decisions and *TD* is the number of total decisions.

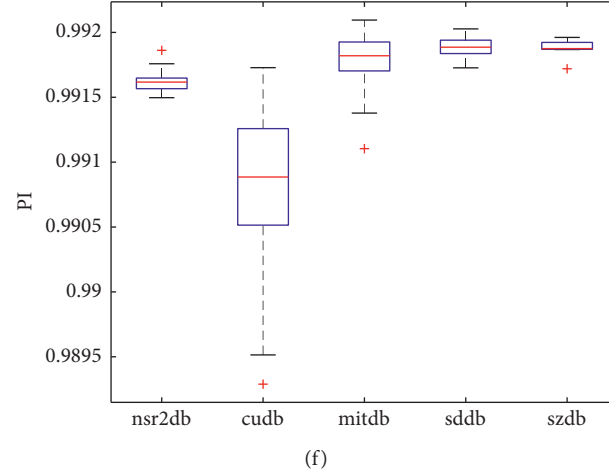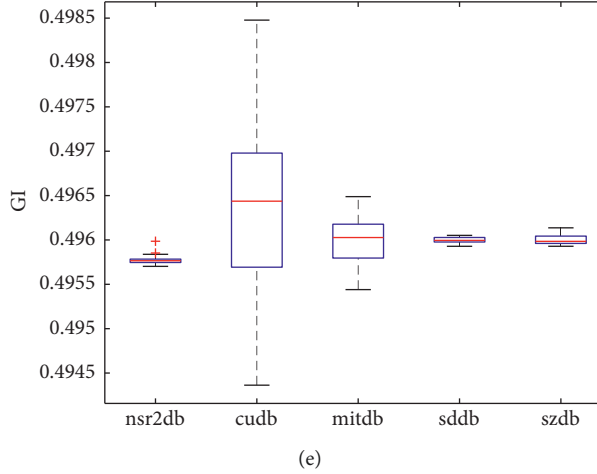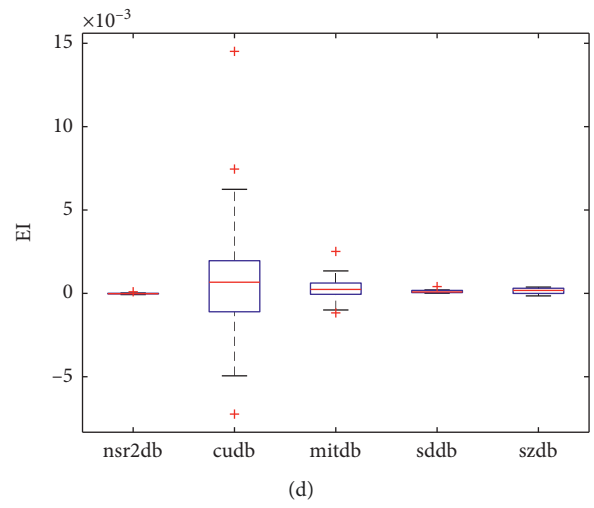Table 3 shows that by comparing the clustering accuracy, the performance of LDE is superior to the six indicators.
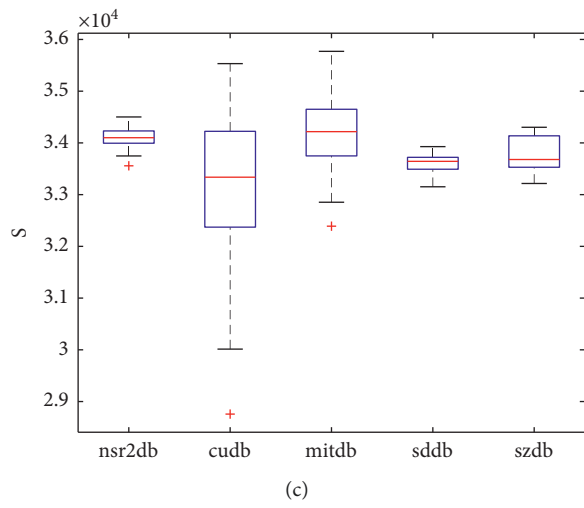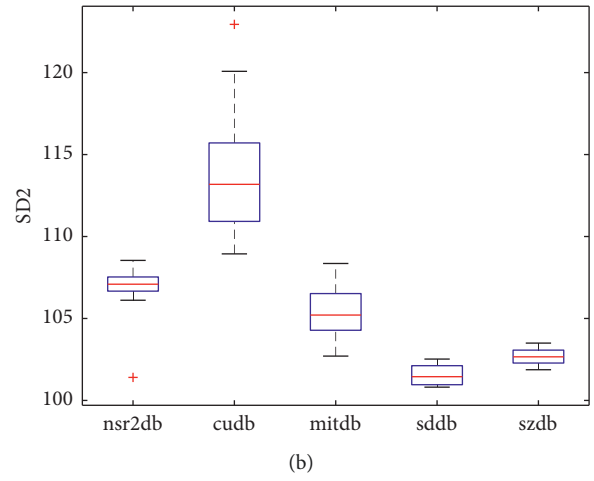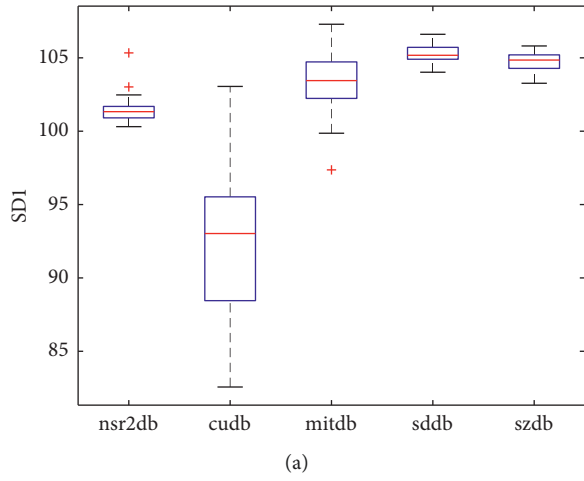
(a)

(b)

(c)
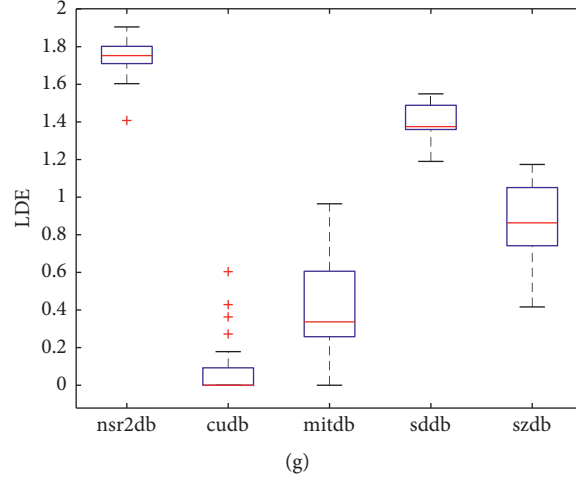
(d)

(e)

(f)

FIGURE 6: Continued.

(g)

FIGURE 6: Results of the seven indicators for the five datasets nsr2db, cudb, mitdb, sddb, and szdb. (a–g) The experimental results of the seven indexes SD1, SD2, S, EI, GI, PI, and LDE, respectively.

TABLE 2: The means and standard deviations of SD1, SD2, S, EI, GI, PI, and LDE.

Indicator	nsr2db	Cudb	Mitdb	Sddb	Szdb
SD1	101.41 ± 0.64	92.73 ± 25.20	103.33 ± 3.82	105.29 ± 0.53	104.72 ± 0.67
SD2	107.06 ± 1.02	113.79 ± 12.09	105.38 ± 2.03	101.55 ± 0.42	102.65 ± 0.31
S	$3.41 \times 10^4 \pm 3.71 \times 10^4$	$3.31 \times 10^4 \pm 2.18 \times 10^6$	$3.42 \times 10^4 \pm 5.12 \times 10^5$	$3.36 \times 10^4 \pm 4.72 \times 10^4$	$3.38 \times 10^4 \pm 1.52 \times 10^5$
EI	$-1.50 \times 10^{-5} \pm 7.35 \times 10^{-10}$	$7.75 \times 10^{-4} \pm 1.47 \times 10^{-5}$	$2.26 \times 10^{-4} \pm 4.12 \times 10^{-7}$	$1.20 \times 10^{-4} \pm 1.31 \times 10^{-8}$	$1.46 \times 10^{-4} \pm 3.69 \times 10^{-8}$
GI	$0.50 \pm 1.91 \times 10^{-9}$	$0.50 \pm 6.79 \times 10^{-7}$	$0.50 \pm 6.63 \times 10^{-8}$	$0.50 \pm 1.43 \times 10^{-9}$	$0.50 \pm 5.0 \times 10^{-9}$
PI	$0.99 \pm 4.94 \times 10^{-9}$	$0.99 \pm 3.60 \times 10^{-7}$	$0.99 \pm 3.99 \times 10^{-8}$	$0.99 \pm 6.25 \times 10^{-9}$	$0.99 \pm 5.89 \times 10^{-9}$
LDE	1.75 ± 0.01	0.07 ± 0.027	0.43 ± 0.06	1.41 ± 0.01	0.85 ± 0.06

TABLE 3: The clustering results of SD1, SD2, S, EI, GI, PI, and LDE.

Indicator	RI			
	nsr2db, cudb	nsr2db, mitdb	nsr2db, sddb	nsr2db, szdb
SD1	0.91	0.80	0.97	0.98
SD2	0.89	0.79	0.97	0.98
S	0.71	0.61	0.91	0.87
EI	0.67	0.60	0.88	0.95
GI	0.82	0.80	0.97	0.98
PI	0.84	0.81	0.95	0.95
LDE	1	1	0.98	1

Therefore, as an effective feature, LDE has the ability to classify cardiovascular diseases.

5. Conclusion

As a useful analysis tool, the Poincaré plot is often used in the heart rate variability analysis, which describes the physiological information of cardiac activity intuitively. To analyze the Poincaré plot, many asymmetry indicators were presented in the literature. However, the temporal relation of the adjacent scatter points is ignored essentially by most classical indicators. To remedy this limitation, a three-dimensional Poincaré plot analysis is presented in the study.

Two main results are obtained in this study. Firstly, a three-dimensional Poincaré plot is presented. In the novel

coordinate system, the z-axis is perpendicular to the plane of the standard Poincaré plot. In a TDPP, the temporal characteristics and the distribution patterns of scatter points can be adequately revealed. Secondly, to analyze the temporal and spatial features of all scatter points quantitatively, local distribution entropy is presented in this study. In the TDPP, the space is divided into several subspaces. By counting the local distribution entropy of all subspaces, we will acquire the physiological information contained in the RR time series.

To further verify the effectiveness of our method, five datasets are applied in this study. The experimental results demonstrate that the spatial–temporal characteristics of the sinus rhythm can be properly described and objectively measured via the three-dimensional Poincaré plot analysis. In addition, to demonstrate the advantage of the method, six

classic indicators of the Poincaré plot are applied. The experimental results illustrate that the three-dimensional Poincaré plot analysis can effectively identify the sinus rhythm from arrhythmia, heart rate oscillations in partial epilepsy, ventricular tachyarrhythmia, and sudden cardiac death. Nevertheless, other indicators only accomplish the recognition tasks partly. These findings indicate that the performance of the three-dimensional Poincaré plot analysis is stable and effective. In the future, LDE can be used as a valuable feature for physiological signal classification.

Data Availability

The data used to support the findings of this study are available at https://www.physionet.org/about/database/.

Conflicts of Interest

The authors declare that there are no conflicts of interest regarding the publication of this paper.

Acknowledgments

References

[1] A. J. Camm, M. Malik, and J. T. Bigger, "Heart rate variability: standards of measurement, physiological interpretation and clinical use. Task force of the european society of cardiology and the north american society of pacing and electrophysiology," *Circulation*, vol. 93, pp. 1043–1065, 1996.

[2] E. H. Hon and S. T. Lee, "Electronic evaluation of the fetal heart rate patterns preceding fetal death, further observations," *American Journal of Obstetrics and Gynecology*, vol. 87, pp. 814–826, 1963.

[3] M. Brennan, M. Palaniswami, and P. Kamen, "Do existing measures of Poincare plot geometry reflect nonlinear features of heart rate variability?" *IEEE Transactions on Biomedical Engineering*, vol. 48, no. 11, pp. 1342–1347, 2001.

[4] M. P. Tulppo, T. H. Makikallio, T. E. Takala, T. Seppanen, and H. V. Huikuri, "Quantitative beat-to-beat analysis of heart rate dynamics during exercise," *American Journal of Physiology - Heart and Circulatory Physiology*, vol. 271, no. 1, pp. H244–H252, 1996.

[5] Z. Xu, J. G. Ge, Q. P. Xu, and H. Zhang, "A quantitative study of Poincare dispersed-dot plot for heart rate variability," *Sheng wu yi xue gong cheng xue za zhi = Journal of biomedical engineering = Shengwu yixue gongchengxue zazhi*, vol. 17, pp. 433–436, 2000.

[6] C. L. Ehlers, J. Havstad, D. Prichard, and J. Theiler, "Low doses of ethanol reduce evidence for nonlinear structure in brain activity," *Journal of Neuroscience*, vol. 18, no. 18, pp. 7474–7486, 1998.

[7] J. Piskorski and P. Guzik, "Geometry of the Poincaré plot ofRRintervals and its asymmetry in healthy adults," *Physiological Measurement*, vol. 28, no. 3, pp. 287–300, 2007.

[8] A. Porta, S. Guzzetti, and N. Montano, "Time reversibility in short-term heart period variability," *Computers in Cardiology*, vol. 33, pp. 77–80, 2006.

[9] A. Kubičková, J. Kozumplík, Z. Nováková, M. Plachý, P. Jurák, and J. Lipoldová, "Heart rate variability analysed by Poincaré plot in patients with metabolic syndrome," *Journal of Electrocardiology*, vol. 49, no. 1, pp. 23–28, 2016.

[10] E. I. Iconaru, M. M. Ciucurel, L. Georgescu, M. Tudor, and C. Ciucurel, "The applicability of the Poincaré plot in the analysis of variability of reaction time during serial testing," *International Journal of Environmental Research and Public Health*, vol. 18, no. 7, p. 3706, 2021.

[11] D. Escutia-Reyes, J. de Jesús Garduño-García, G. Emilio-López-Chávez et al., "Differences in heart rate variability and body composition in breast cancer survivors and women without cancer," *Scientific Reports*, vol. 11, no. 1, Article ID 14460, 2021.

[12] R. Shashikant, U. Chaskar, L. Phadke, and C. Patil, "Gaussian process-based kernel as a diagnostic model for prediction of type 2 diabetes mellitus risk using non-linear heart rate variability features," *Biomedical Engineering Letters*, vol. 11, no. 3, pp. 273–286, 2021.

[13] M. C. Stoco-Oliveira, A. L. Ricci-Vitor, L. M. Vanzella et al., "Parkinson's disease effect on autonomic modulation: an analysis using geometric indices," *Arquivos de Neuro-Psiquiatria*, vol. 79, no. 2, pp. 114–121, 2021.

[14] D. G. Goroso, W. T. Watanabe, F. Napoleone et al., "Remote monitoring of heart rate variability for obese children," *Biomedical Signal Processing and Control*, vol. 66, Article ID 102453, 2021.

[15] S. R. Rathod and C. Y. Patil, "Statistical validity of presmoking and postsmoking impact on heart rate variability among middle age men," *Lecture Notes in Electrical Engineering*, vol. 703, pp. 271–277, 2021.

[16] C. Diao, A.-H. Zhang, and B. Wang, "Spectral clustering with local projection distance measurement," *Mathematical Problems in Engineering*, vol. 2015, pp. 1–13, 2015.

[17] X. Yang, L. Liao, Q. Yang, B. Sun, and J. Xi, "Limited-energy output formation for multiagent systems with intermittent interactions," *Journal of the Franklin Institute*, vol. 358, no. 13, pp. 6462–6489, 2021.

[18] J. Jin, J. Li, D. Qin, and N. Cai, "Output formation tracking for networked systems with limited energy and aperiodic silence," *Chinese Journal of Aeronautics*, 2021.

[19] C. Diao, B. Wang, and N. Cai, "Data fusion of multivariate time series: application to noisy 12-lead ECG signals," *Applied Sciences*, vol. 9, no. 1, p. 105, 2018.

[20] J. Xi, L. Wang, J. Zheng, and X. Yang, "Energy-constraint formation for multiagent systems with switching interaction topologies," *IEEE Transactions on Circuits and Systems I: Regular Papers*, vol. 67, no. 7, pp. 2442–2454, 2020.

[21] F. Takens, "Detecting strange attractors in turbulence," *Lecture Notes in Mathematics*, vol. 898, pp. 366–381, 1981.

[22] A. L. Goldberger, L. A. N. Amaral, L. Glass et al., "PhysioBank, PhysioToolkit, and PhysioNet," *Circulation*, vol. 101, no. 23, pp. 215–220, 2000.

[23] G. B. Moody and R. G. Mark, "The impact of the MIT-BIH arrhythmia database," *IEEE Engineering in Medicine and Biology Magazine*, vol. 20, no. 3, pp. 45–50, 2001.

[24] I. C. Al-Aweel, K. B. Krishnamurthy, J. M. Hausdorff et al., "Postictal heart rate oscillations in partial epilepsy," *Neurology*, vol. 53, no. 7, 1590 pages, 1999.